Co and Fe co-doping influence on functional properties of SrTiO₃ for use as oxygen transport membranes

Yang Liua,*, Stefan Baumanna, Falk Schulze-Küppersa, David N. Muellerb, Olivier Guillona

Abstract

Perovskite-structured powders of $SrTi_{1-x}Co_xO_{3-\delta}$ (STC-x) with nominal stoichiometry of x=0-0.75 as well as $SrTi_{0.75}Co_{0.25-y}Fe_yO_{3-\delta}$ (STCF-y) where y=0-0.25 were synthesized using the Pechini method. Thermal/chemical expansion behaviour, total electrical conductivities, and oxygen permeation rates were investigated. The substitution of Ti with Co leads to an increase in both electronic and ionic conductivities and, therefore, oxygen permeability. Thermal and chemical expansions also increase slightly. The optimum Co content was found to be 25-35% due to the trade-off between phase stability and permeability. The oxygen permeation rate of STC35 is comparable to that of state-of-the-art (La,Sr)(Co,Fe)O_{3-\delta}, whereas the expansion coefficients are lower. Co-doping in STCF-y did not produce any significant differences in oxygen permeability at both high temperature and sample thickness (1.0 mm), i.e. in a solid-state diffusion-limited regime. At lower temperatures (<800 °C), STC25 exhibits higher permeability than STF25 due to the higher catalytic activity of Co compared to Fe.

Keywords: Oxygen transport membrane, cobalt doping, strontium titanate, conductivity, permeance

1. Introduction

Mixed ionic and electronic conductors (MIEC) have gained much attention due to their potential application in oxygen transport membranes to separate oxygen from air or other oxygen-containing gas mixtures as well as their potential application on membrane reactors for partial

^a Forschungszentrum Jülich GmbH, Institute of Energy and Climate Research – Materials Synthesis and Processing (IEK-1), Leo-Brandt-Strasse, 52425 Jülich, Germany

^b Forschungszentrum Jülich GmbH, Peter Grünberg Institute – Electronic Properties (PGI-6), Leo-Brandt-Strasse, 52425 Jülich, Germany

oxidation, for example syngas production [1, 2]. Moreover, MIEC perovskites are used in electrochemical devices such as solid oxide fuel cell (SOFC) electrodes, particularly cathodes [3, 4]. One promising class of membrane materials are the cubic perovskites ABO_{3-δ}, with the A cation at the corner of the cube and the B cation in the centre of the cubic unit cell with oxygen ions in the face-centred positions, leading to the formation of BO6 octahedra extended three dimensionally. The cubic perovskite structure materials have the advantage of accommodating a number of different cations with different valences in its lattice. In other words, different elements can be doped on the A site or B site to obtain different oxygen stoichiometries, facilitating the formation of oxygen vacancies and electron holes to achieve the desired MIEC behaviour [5]. The SrFeO_{3-ō}- and SrCoO_{3-ō}-based perovskite materials with A site substitutions such as Ba and La were comprehensively investigated. Among them, the La_{1-x}Sr_xCo_yFe_{1-y}O_{3-\delta} (LSCF), SrCo_{0.8}Fe_{0.2}O_{3-\(\delta\)}, and Ba_{0.5}Sr_{0.5}Co_{0.8}Fe_{0.2}O_{3-\(\delta\)} (BSCF) series were reported to have a high oxygen permeation rate [6-10]. However, LSCF and BSCF have low phase stabilities in low oxygen partial pressures [11-13] as well as aggressive gases such as CO, CH₄, and CO₂ [14]. Therefore, B-site doping by Zr, Nb, Ti, and Y, particularly in BSCF, was carried out to improve stability [15-22]. These approaches were successful to a certain extent, but the large amount of Co and Fe in the B site of these materials still leads to limited resistance in reducing environments. In contrast, research was carried out on the perovskite material SrTiO₃, which is chemically and structurally very stable but practically impermeable to oxygen. By introducing a limited amount of multivalent Fe into the B site sublattice of TiO₆ octahedra, oxygen vacancies and electron holes are formed, thus leading to an oxygen permeation rate comparable to LSCF [23].

Figure 1 shows a schematic quasi-ternary phase diagram of SrCoO₃, SrFeO₃, and SrTiO₃. The black dots in the diagram (Figure 1) represent compositions that were reported in the literature. The quasi-binary system SrCoO₃-SrFeO₃ (SCF) [24, 25] has evidently been comprehensively investigated, including limited B site substitution by Ti [26-30]. Furthermore, the quasi-binary system SrFeO₃-SrTiO₃ (STF) has also been studied [23, 31-34]. The quasi-binary system SrTiO₃-SrCoO₃ (STC) region with high Ti content has been widely investigated with respect to magnetic properties [35-41]. However, the use of mixed ionic and electronic conductivity for oxygen transport membrane (OTM) materials has not yet been systematically characterized. However, it is known that Co is more effective than Fe in terms of the functionalization of perovskites [42, 43]. Therefore, in this paper, compositions of SrTi_{1-x}Co_xO_{3-ō} (STC-x) where x=0, 0.05, 0.15, 0.25, 0.35, 0.5, and 0.75 and compositions of SrTi_{0.75}Co_{0.25-y}Fe_yO_{3-ō} (STCF-y) where y=0, 0.06, 0.125, and 0.19 were investigated in terms of their functional and manufacturing properties (open dots in

Figure 1). The effect of Co doping and Fe/Co co-doping in STO on oxygen permeation, electrical conductivity, and thermal/chemical expansion behaviour is discussed.

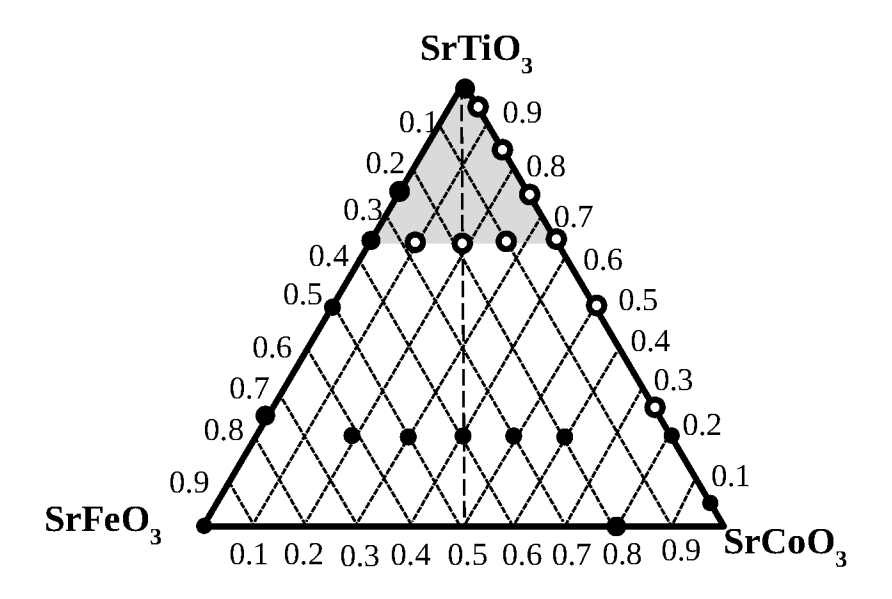


Figure 1 Quasi-ternary diagram of SrTiO₃, SrFeO₃, and SrCoO₃ showing the compositions investigated in the literature (full circles) and in this study (open circles), respectively [24-29].

2. Experimental

2.1 Powder preparation

SrTi_{1-x}Co_xO_{3-δ} (x=0.05, 0.15, 0.25, 0.35, 0.5, 0.75) and SrTi_{0.75}Co_{0.25-y}Fe_yO_{3-δ} (y=0.06, 0.125, 0.19) powders were prepared using the Pechini synthesis method. Firstly, Ti⁴⁺ aqueous solution stabilized with nitric acid was obtained by removing the organic part of Titanium(IV) isopropoxide (Ti[OCH(CH₃)₂]₄) (Sigma Aldrich) in deionized water. Sr(NO₃)₂, Co(NO₃)₂.6H₂O, and Fe(NO₃)₃.9H₂O (Merck KGaA) were dissolved in deionized water and the stabilized Ti⁴⁺ aqueous solution was added. Citric acid (Merck KGaA) was also added for complexation and ethylene glycol (Merck KGaA) was added for polymerization. After polymerization and the evaporation of water from the solution, the formed gel was heated at 600 °C to remove the organic compounds. The powders were then calcined at 950 °C for 5h to obtain the pure cubic perovskite phase.

In order to achieve a powder with monomodal and narrow particle size distribution, all calcined powders were milled in ethanol with 3 mm ZrO_2 balls for 24h. The weight ratio of the powder, ethanol, and balls was 1: 2: 3. The dry powder agglomerates were subsequently crushed in an Agate mortar and sieved through a 200 μ m mesh.

The as-prepared powder was then pressed to be sintered at different temperatures ranging from 1280 °C to 1400 °C, dwelling for 10h to achieve relative densities higher than 98%. Sintering parameters of the samples are shown in Table 1.

2.2 Characterization

The chemical compositions of the synthesized powders calcined at 950 °C were measured by inductively coupled plasma optical emission spectrometry (ICP-OES). Specific surface areas of the calcined and ball-milled powders were determined in an AreaMeter (Ströhlein, Germany) by nitrogen adsorption and particle size distribution by laser granulometry using a Horiba LA-950V2 device. The phase composition of the calcined powder was characterized by X-ray powder diffraction (XRD) (D4 ENDEAVOR diffractometer by Bruker XS with CuKα radiation (λ=1.54 Å)). In addition, the morphology of the as-prepared powder was characterized by means of scanning electron microscopy (Zeiss Ultra55).

The relative density of the sintered samples was measured using the method of Archimedes. In order to investigate the thermal/chemical expansion behaviour of sintered samples, 25-mm-long sintered-bar-shaped samples were tested in a Netzsch 402C dilatometer with a heating and cooling rate of 3 °C/min up to 1000 °C in synthetic air using F_{air}= 100 ml/min. Electrical conductivities of the STC-x and STCF-y samples were determined using the 4-point-probe conductivity method in the temperature range of 650 °C to 875 °C. Oxygen permeation measurements of 1.0-mm-thick disc-shaped membranes with a 14.7 mm diameter were conducted in air/Ar oxygen partial pressure gradients at a constant flow rate of 250 ml/min of ambient air as a feed gas and 50 ml/min of Ar as a sweep gas, as was reported elsewhere [23]. The temperature was varied between 1000 °C and 650 °C. Samples were ground with P1200 emery paper prior to oxygen permeation measurements to remove possible contaminations from sintering and to provide a defined thickness and comparable surface roughness. Gold rings with an inner diameter of 13 mm were used to seal the samples to the gasket of the quartz glass reactor at approx. 1000 °C, resulting in an exposed membrane surface area of approx. 1.33 cm².

3. Results and Discussion

3.1 Powder characterization

The particle size distribution, specific surface area, and lattice parameters of the calcined (950 $^{\circ}$ C) powders as well as the sintering temperature required to obtain highly dense samples (>98% of theoretical density) are shown in Table.1. The d₅₀ values are around 2 μ m and the specific surface

areas are around 1-5 m^2/g . ICP-OES results (not shown here) confirmed the desired composition of Sr, Ti, Co, and Fe.

Table 1 Particle size distribution, specific surface area of processed powder, and sintering temperature of the samples.

Name	Composition	d ₁₀ μm	d ₅₀ μm	d ₉₀ µm	Spec. surface area m²/g	Sintering temperature (°C)
STC05	SrTi _{0.95} Co _{0.05} O _{3-δ}	0.39	2.53	7.13	1.4	1400
STC15	SrTi _{0.85} Co _{0.15} O _{3-δ}	0.84	2.43	6.61	2.4	1400
STC25	SrTi _{0.75} Co _{0.25} O _{3-δ}	0.89	2.68	6.38	4.4	1280
STC35	SrTi _{0.65} Co _{0.35} O _{3-δ}	0.79	2.21	5.93	4.5	1250
STCF19	SrTi _{0.75} Co _{0.06} Fe _{0.19} O _{3-б}	0.68	1.99	4.91	5.7	1300
STCF12.5	SrTi _{0.75} Co _{0.125} Fe _{0.125} O _{3-δ}	0.64	2.16	5.789	3.4	1300
STCF6	SrTi _{0.75} Co _{0.19} Fe _{0.06} O ₃₋₅	0.63	2.35	5.65	4.4	1300

Figure 2 shows SEM images of the calcined STC25 and STCF12.5 powders, which are representative of all powders. The images reveal that the powders consist of dense agglomerates of nanosized primary particles, which is typical for the Pechini method.

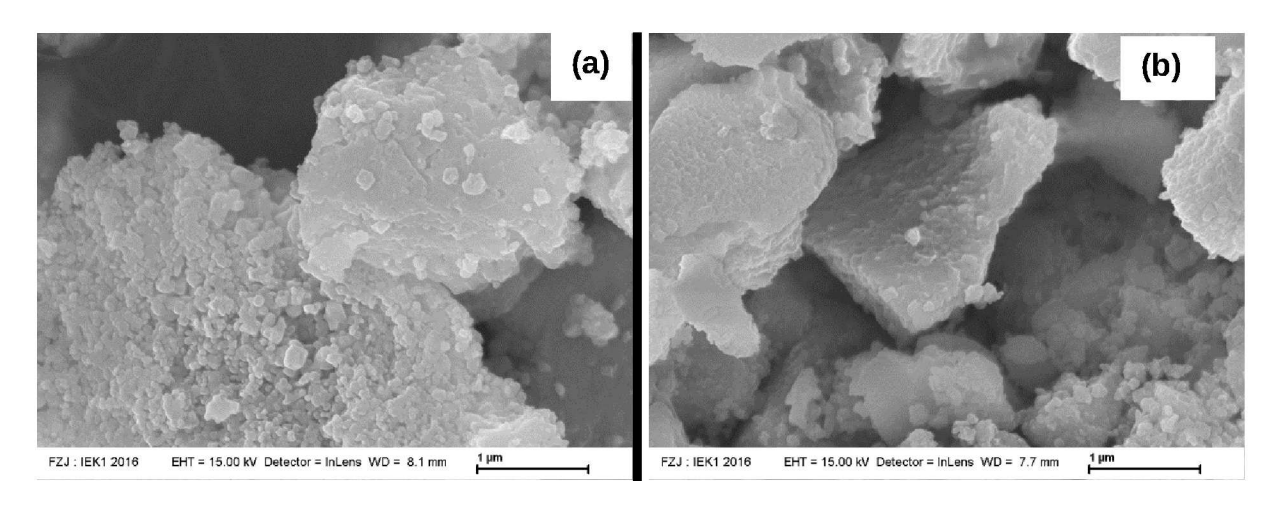


Figure 2 SEM images of the (a) STC25 and (b) STCF12.5 powder.

XRD patterns of the powders calcined at 950 °C where $x \le 0.50$ indicate a perovskite structure, as shown in Figure 3, whereas in a high Co concentration where x > 0.5, the STC-x material exhibited a secondary phase in addition to the perovskite structure. Furthermore, samples with a high Co content ($x \ge 0.5$) showed instability in ambient air at room temperature, since they cracked easily in the short term, i.e. within just a few days. STC-x where $x \ge 0.5$ was therefore excluded from the following investigations.

The lattice parameters determined by Rietveld refinements are plotted in Figure 4 and follow Vegard's law [44]. The lattice parameters of the STC-x materials were in good agreement with the literature [36, 39, 45]. The lattice parameter in STC-x decreased slightly due to the doping of cobalt in the B site of SrTiO₃ (STO). At a constant total B site substitution of 25% in STCF-y, the lattice parameter increases with increasing iron content. This can be explained by the ionic size decreasing in the order of Ti⁴⁺>Fe³⁺>Co³⁺ in the octahedral configuration [46].

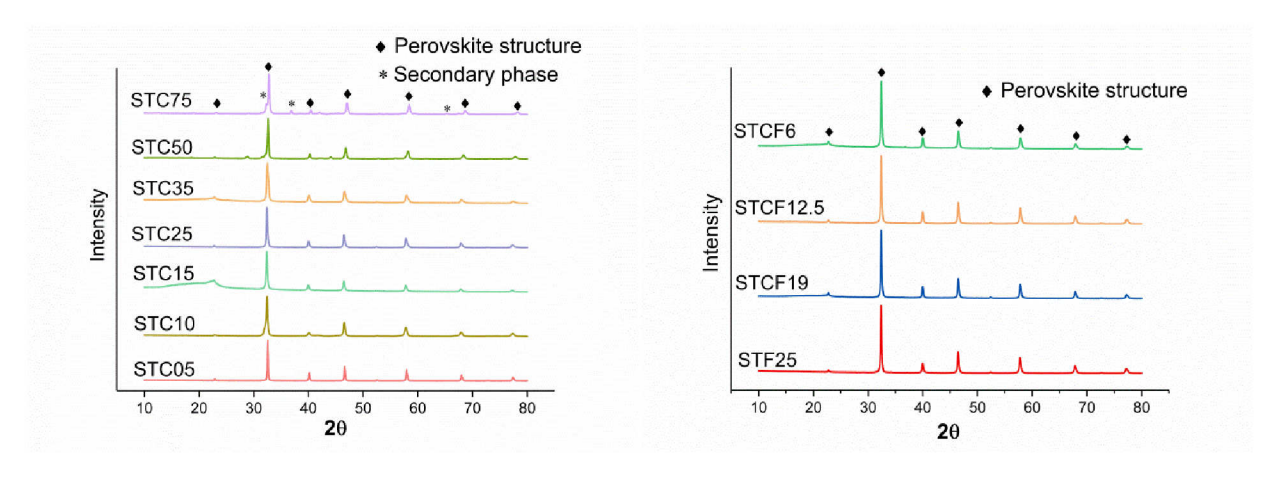


Figure 3 XRD patterns of the powders calcined at 950 °C.

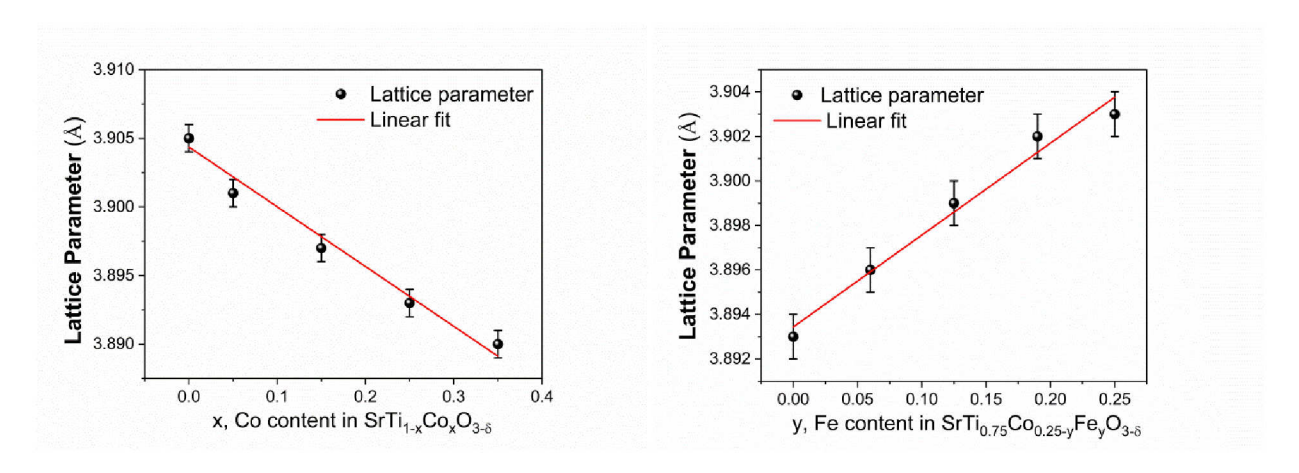


Figure 4 Lattice constant vs. Co content in $SrTi_{1-x}Co_xO_{3-\delta}$ (x=0.05, 0.15, 0.25, 0.35) and Fe content in $SrTi_{0.75}Co_{0.25-v}Fe_vO_{3-\delta}$ (y=0.06, 0.125, 0.19, 0.25).

The samples were sintered at different temperatures ranging from 1250 °C to 1400 °C in order to obtain high densities as shown in Table.1. This might lead to differences in microstructure in particular grain size. Therefore, SEM images were taken from fractured surfaces of STC05, STC35 and STCF12.5 representative for the entire variation in composition and sintering temperature. As shown in Figure 5, in all cases the fracture occurs partly in transgranular and intergranular mode. Nevertheless, it is clearly visible that the grains are comparable in size of approx. 1-2 μ m. In a former study using BSCF an even larger variety of grain sizes was investigated showing no influence on oxygen permeation[47]. Hence, the influence of sintering temperature of STC and STCF on functional properties is considered negligible.

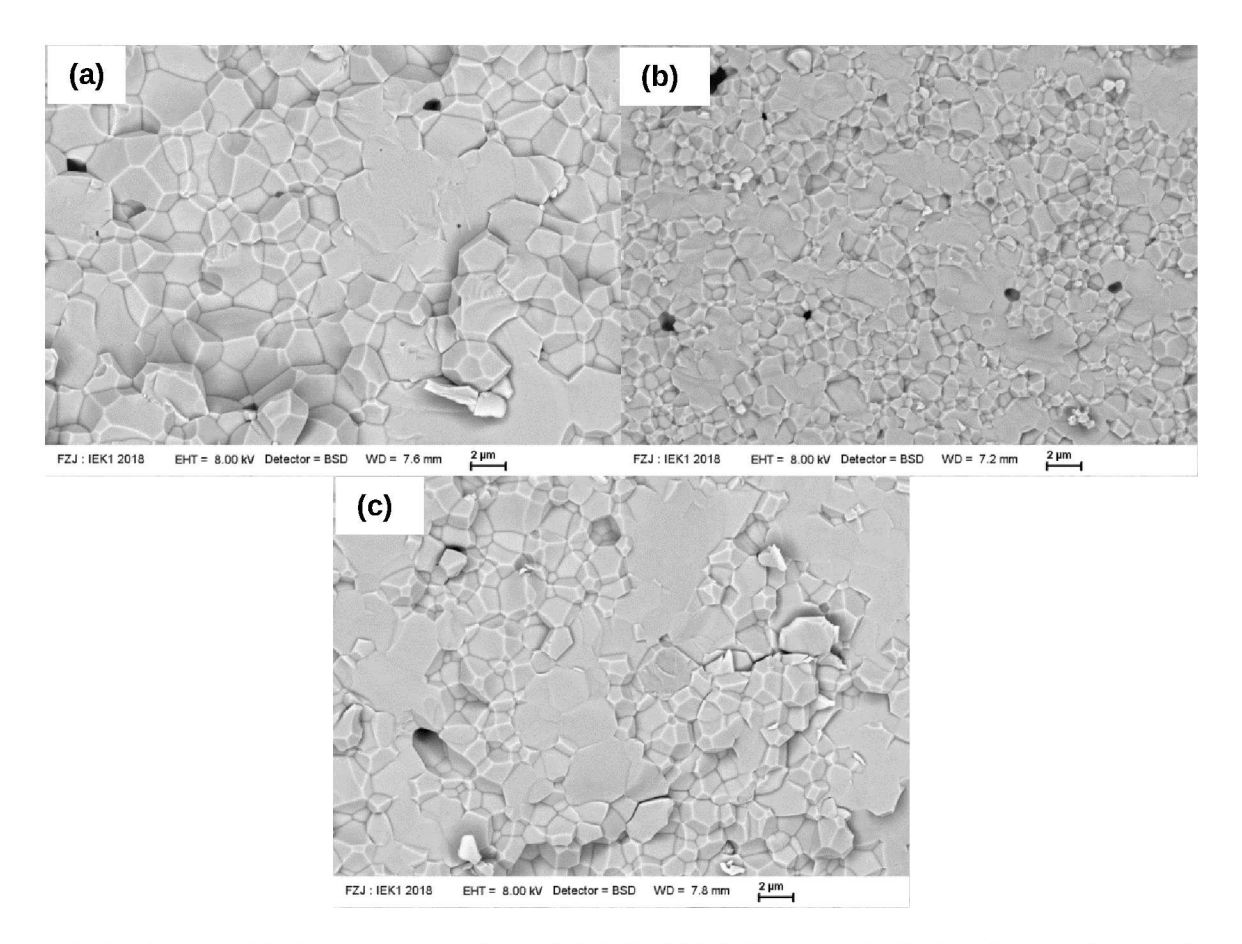


Figure 5 SEM images of the fracture surface of the (a) STC05, (b) STC35, and (c) STCF12.5 after sintering at 1400 °C, 1250 °C, and 1300 °C, respectively.

3.2 Thermal expansion

Dilatometric measurements in air and Ar, respectively, were performed from RT to 1000 °C in order to investigate the expansion behaviour of the studied materials. The total expansion of the mixed ionic electronic conductor in air is composed of thermal expansion and chemical expansion. Thermal expansion is caused by the increase in the average distance between lattice ions with increasing temperature. In contrast, chemical expansion is mainly associated with the release of oxygen from the lattice and the corresponding reduction of the multivalent Co or Fe ions on the B site. As a result, total expansion increased with decreasing p_{02} , i.e. Ar atmosphere during heating, whereas the uptake of oxygen is very limited during cooling due to the low p_{02} . Therefore, the contraction process in an argon atmosphere during cooling can be used to determine the pure thermal expansion coefficient, whereas the chemical expansion coefficient α_{chemical} can be determined using the difference between the total and thermal expansions [48]. The expansion coefficients of STC-x and STCF-y in the temperature range of 60 °C to 1000 °C are listed in Table

2. The total expansion coefficients increased significantly with the increase of Co concentration in STC-x due to enhanced $\alpha_{thermal}$ and $\alpha_{chemical}$. The increase of $\alpha_{chemical}$ is due to the higher Co content leading to more vacancy formation whereas the increase of $\alpha_{thermal}$ might be caused by weaker bonds of Co-O compared to Ti-O.

It is worth noting that the total expansion coefficient of STC35 (16.9*10⁻⁶ K⁻¹), the highest among the studied materials, is still below that of standard perovskites such as LSCF and BSCF (17.4 and 19.6 [10⁻⁶ K⁻¹], respectively) and is therefore in better agreement with that of possible metallic supports or frames, e.g. Hastelloy X (16.5*10⁻⁶ K⁻¹) [49]. The thermal expansion of constant B site doping STCF-y decreases slightly with increased y, whereas the chemical expansion is identical. This might be because Fe does not lead to any significantly different amount of oxygen vacancy formation compared to Co, but the Fe-O bond is a bit stronger compared to Co-O.

Figure 6 shows the expansion of STC25 in air and Argon during heating and cooling. It should be noted that during the heating process, the expansion rate becomes slower at 900 °C for a high B site doping content, i.e. ≥25%. However, this tiny change is expected to have a minor effect in the engineering application.

Table 2 Expansion coefficients in (10⁻⁶ K⁻¹) of STC-x and STCF-y materials calculated from the cooling branches between 1000 °C and 60 °C; STO data were taken from the literature [23].

Sample	STO	STC05	STC15	STC25	STC35	STCF19	STCF12.5	STCF6
α _{total}	11.6	13.0	14.4	15.5	16.9	14.0	14.3	14.8
$lpha_{ ext{thermal}}$	11.6	12.9	14.0	14.7	15.4	13.2	13.5	14.0
$lpha_{ ext{chemical}}$	0	0.1	0.4	0.8	1.5	0.8	0.8	0.8

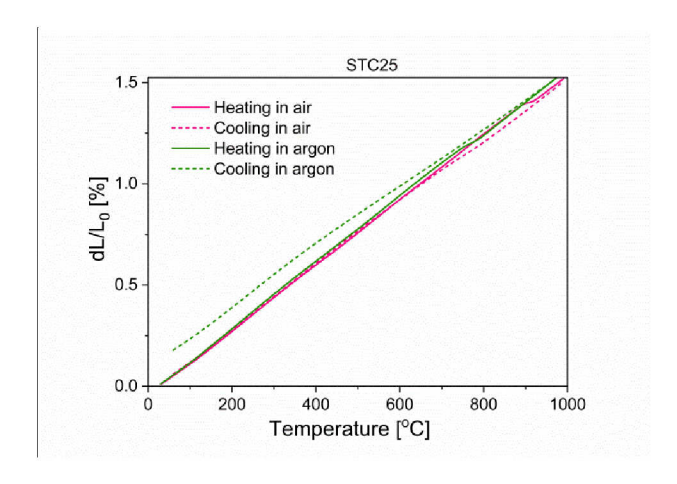


Figure 6 Dilatometric curves of STC25 in air and in argon.

3.3 Electrical conductivity

The total conductivity (σ_t) is generally given by the sum of ionic (σ_i) and electronic conductivities (σ_e) [50, 51]. The electronic conductivity of the STC is caused by the hopping of electronic charge carriers between the cations of different valences, such as Co^{2+} and Co^{3+} . On the other hand, the ionic conductivity is a result of the oxygen vacancies that form for electroneutrality due to the $Co^{2+/3+}$ substitution of Ti^{4+} in the B-site [52]. In this study, the conductivity determined by 4-probe DC measurements is the total conductivity. The dashed lines in Figure 7 represent linear fits according to an Arrhenius behaviour:

$$\sigma_t = \sigma_0 \cdot \exp(-\frac{E_a}{RT}) \tag{1}$$

Since the ionic conductivity of MIEC for OTMs is typically orders of magnitude smaller compared to the electronic conductivity in air [1, 43, 53], the total conductivity value can be considered as the electronic conductivity. Total conductivity increases with temperature in the studied temperature range (650 °C to 875 °C) in air. Conductivity increased notably with an increase in the concentration of Co, whereas the activation energy Ea calculated using the Arrhenius equation decreased with Co concentration. The band gap energy for the mobility of defects decreased due to Co doping, which facilitates the hopping of the electron holes and electrons [54]. It is obvious that the conductivity of STC25 is higher than that of STF25. As expected, Co doping facilitates electronic conductivity more effectively than Fe, which is consistent with the literature [24, 43, 55, 56]. In the STCF-y system, the total dopant concentration in the B site is kept constant at 25%. Electronic conductivity remains relatively constant at a high Fe content until an equal mixture of Fe and Co (12.5% each). A further decrease in Fe concentration, and therefore an increase in Co concentration, leads to jumps in conductivity, whereas the activation energy remains constant.

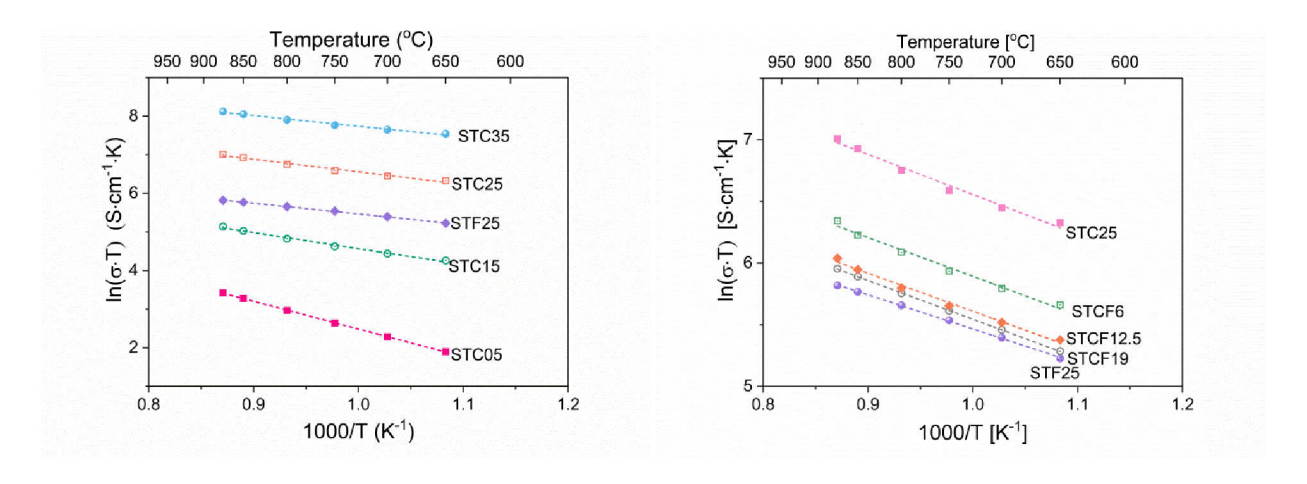


Figure 7 Arrhenius plot of the total conductivity of a) the STC-x series and b) the STCF-y series. The dashed lines are linear fits according to Arrhenius law.

Figure 8a shows the dependence of conductivity on Co concentration. Above 15% cobalt, there is a stronger increase in conductivity with increasing cobalt concentration compared to lower levels of cobalt substation. At the same time, the activation energy also shows a kink in the behaviour, as shown in Figure 8b. This points to a change in the conduction mechanism, which was similarly observed in the LSCF series [24]. At a critical concentration of Co, a percolating network of CoO_6 octahedra is formed, meaning that the participation of Ti in the conduction mechanism is not necessary. If the reference transition metal cation is defined as Co_{Co}^{x} , the hole responsible for the electronic conductivity would be trapped at the Ti site as Ti_{Co}^{x} . However, since the 3d levels of Ti and Co differ more significantly in energy with respect to the Fermi level than Fe and Co – owing to their positions in the periodic table – the effect is much more pronounced here.

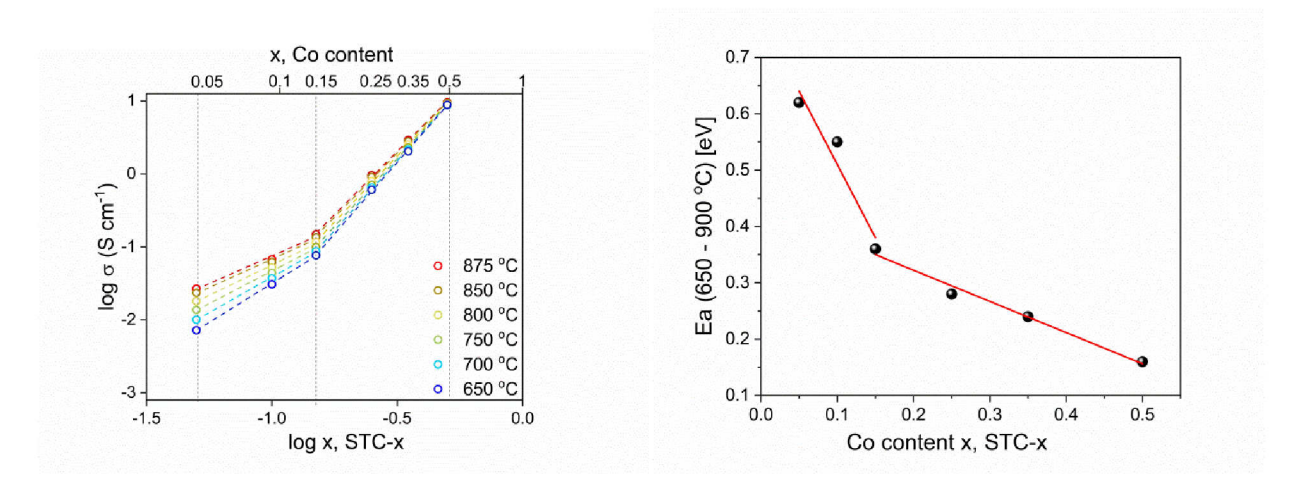


Figure 8 a) total conductivity and b) respective activation energies as a function of the cobalt content.

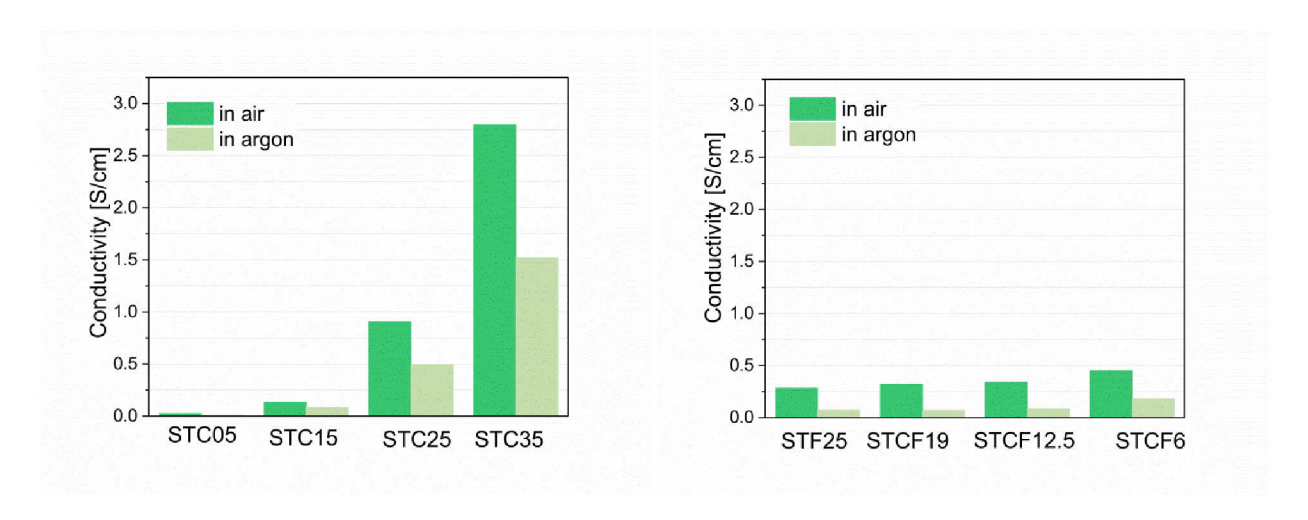


Figure 9 Conductivity of (a) STC-x and (b) STCF-y in air and argon at 850 $^{\circ}$ C

In addition, the conductivity of the studied materials was measured in an Ar atmosphere (p_{O2} about 10^{-5} bar), as shown in Figure 9. The conductivity in argon decreased compared to in air, thus indicating p-type conductivity in this range of p_{O2} , which is consistent with the literature on STF [33, 54, 57].

3.4 Oxygen permeation

The oxygen permeation rate depends on the driving force, i.e. gradient of oxygen partial pressures at both sides of the membrane $\ln\frac{p'_{O_2}}{p''_{O_2}}$, according to equation (2). However, in the measurement, p''_{O_2} is dependent on the accumulation of permeated oxygen in the sweep gas, which suggests that the driving force varies with temperature. In equation (2), solid-state diffusion is assumed to be the rate-limiting step, which is typically the case when using samples of 1.0 mm thickness, as is the case in this study.

In order to confirm this assumption, the permeation rate of STC25 was measured in dependence of the thickness L, i.e. 0.5 mm, 1.0 mm, and 1.5 mm. Figure 10 shows proportionality of the permeation rate with the reciprocal thickness as expected from equation (2) confirming validity of the Wagner model in the investigated materials system.

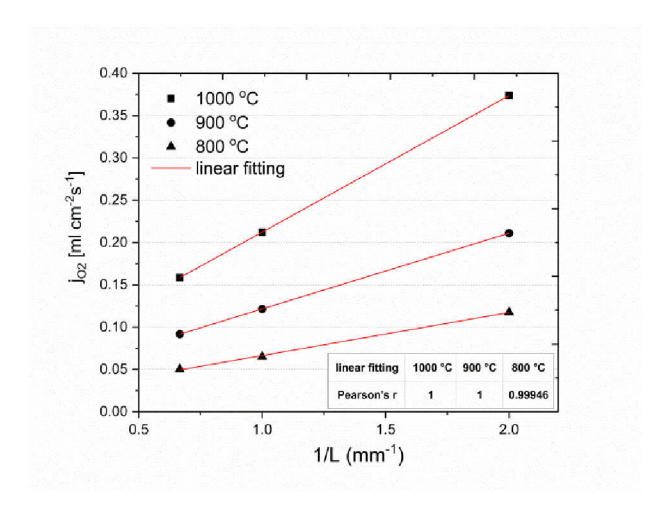


Figure 10 Permeation rate of STC25 sample in terms of reciprocal membrane thickness.

In order to compare the different materials, the permeance, i.e. the driving force normalized permeation rate according to the IUPAC recommendation, is therefore used in the following [58]:

$$j_{O_2} = \frac{RT}{16F^2} \cdot \sigma_{amb} \cdot \frac{1}{L} \cdot \ln \frac{\rho'_{O_2}}{\rho''_{O_2}}$$
 (2)

$$\sigma_{amb} = \frac{\sigma_i * \sigma_e}{\sigma_i + \sigma_e} \tag{3}$$

Permeance =
$$\frac{j_{O_2}}{\ln \frac{\rho'_{O_2}}{\rho''_{O_2}}} = \frac{R}{16F^2} \frac{1}{L} \cdot \sigma_{amb} \cdot T$$
 (4)

where R is the gas constant, T the absolute temperature, F the Faraday constant, σ_{amb} the ambipolar conductivity, L the thickness of the membrane, and ρ'_{O_2} and ρ''_{O_2} the oxygen partial pressures on the oxygen-rich side and oxygen-lean side, respectively.

As expected, the permeation rate increases with Co content (Figure 11). STC35 exhibits a comparable permeation rate to the standard OTM material LSCF6428 at 900 °C, and is higher at lower temperatures (< 900 °C) due to lower activation energy E_a . According to equation (4), the activation energy of the permeance is equal to that of $\sigma_{amb} \cdot T$. An increase in E_a at lower temperatures, which was especially observed in STC15 indicates a change in transport mechanism. Typically this is attributed to the influence of oxygen surface exchange [59]. Figure 12 shows the dependence of E_a on the total B site substitution using Co (in this study) or Fe determined from comparable measurements in our previous work [23]. As described in section 3.4, the activation energy and, therefore, the transport mechanism of the total conductivity are different at low and high substitution levels and changes at around 25%. Similar to the total conductivity, it appears that a minimum substitution threshold (around 15-25%) is necessary to

induce sufficient transport of both ionic and electronic charge carriers and, hence, oxygen permeation. The STCF-y series with a constant B site substitution of 25% does not show any significant change in either the permeation rate or E_a (~101±4 kJ/mol) at high temperatures, as shown in Figure 13. At lower temperatures, it becomes evident that an increase in E_a , which indicates an initial influence of surface exchange limitations, is most pronounced for STF25, followed by the three STCF solid solutions, and is least pronounced for STC25. This is explained by the high catalytic activity of Co in the B site of perovskites [60, 61]. The slightly lower activation energy of STC25 compared to the other materials from the STCF-y series supports this hypothesis.

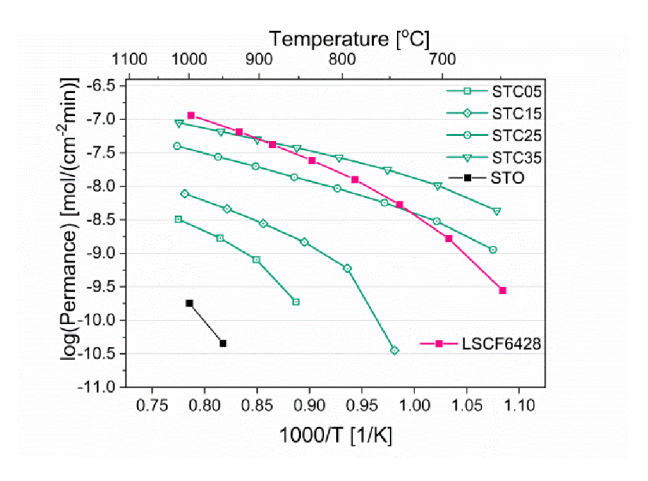


Figure 11. Arrhenius plot of the permeance of the STC-x series measured from 1.0-mm-thick pellets; STO and LSCF6428 was taken from the literature [23].

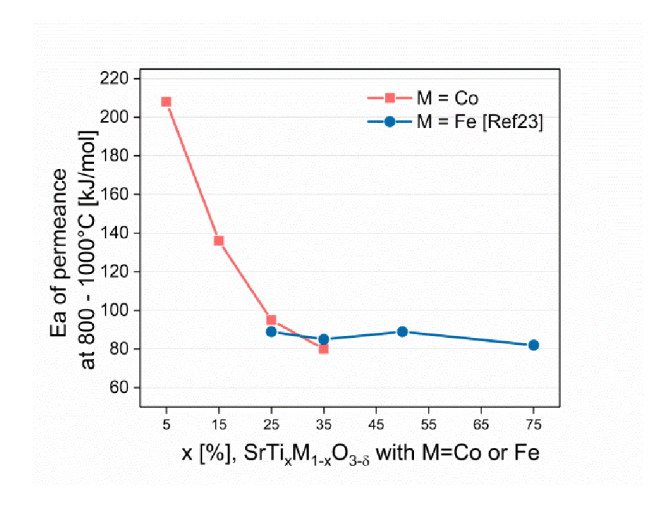


Figure 12. High temperature activation energy of $SrTi_{1-x}M_xFe_{3-\delta}$ where M=Co and M=Fe.

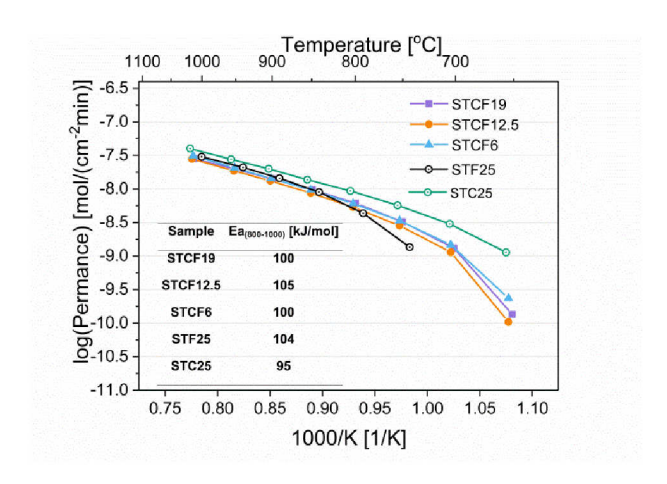


Figure 13. Arrhenius plot of the permeance of the STCF-y series with constant B site substitution of 25%

In order to investigate the surface exchange sensitivity of STC25 and STF25 in particular at the lower temperature range, i.e. 600 - 800 °C, samples of 0.5 mm thickness were measured with and without porous LSCF activation layers on both sides of the membranes, Figure 14. Indeed, the activation layers show no influence on the permeation rate of the STC25 sample except at the lowest temperature of 650 °C indicating bulk diffusion as main transport mechanism in these conditions even at relatively low thickness and temperature. In contrast, for STF25 the activation layers are effective already below 800 °C indicating severe suce limitations at 0.5 mm thickness and low temperatures. At 650°C the difference is around one order of magnitude.

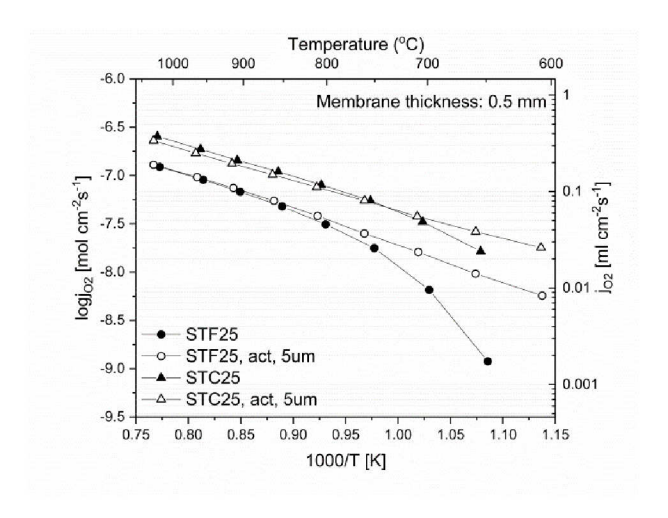


Figure 14. Permeation rate of STC25 and STF25 of 0.5 mm thickness with and without ~5 um thick LSCF surface activation layers.

The ambipolar conductivity of the STCF-y materials calculated from equation (4) at 850 °C is listed in Table 3. σ_{amb} is around two orders of magnitude lower than σ_t , but exhibits a similar trend in terms of substitution level, which is consistent with the literature [59, 62]. It is assumed that the electronic conductivity is higher than the ionic conductivity, as is known from related perovskite MIEC materials [1, 43, 53]. Ionic and electronic conductivities can therefore be calculated from σ_{amb} and σ_t using equation (3), listed in Table 3. The results show that σ_{amb} is close to σ_i , whilst σ_t is close to σ_e . The ionic conductivity of STC35, for example, is 0.06 S/cm at 850 °C. This is comparable to the typical ionic conductor yttria-stabilized zirconia (8YSZ) ($10^{-2} \sim 10^{-1}$ S/cm at 800 °C to 1000 °C) [63-65].

Table 3. Conductivities and ionic transference number of STC-x and STCF-v at 850 ℃.

	STC05	STC15	STC25	STC35	STC6F19	STC12.5F12.5	STC19F6	STF25
σ _{amb} [S/cm]	0.0003	0.002	0.022	0.060	0.016	0.014	0.015	0.014
$\sigma_t \\ [\text{S/cm}]$	0.023	0.14	0.91	2.8	0.32	0.34	0.45	0.28
$\sigma_{i} \\ [\text{S/cm}]$	0.0003	0.002	0.022	0.06	0.016	0.014	0.015	0.015
$\sigma_{\rm e} \\ [\text{S/cm}]$	0.023	0.14	0.89	2.74	0.30	0.33	0.43	0.27

The respective ionic transference numbers t_i can be calculated according to equation (5):

$$t_i = \frac{\sigma_i}{\sigma_t} \tag{5}$$

Figure 15 clearly shows that ionic conductivity increases linearly with the total conductivity in the STC-x series at 850 °C, thus indicating a constant t_i. In contrast, the STCF-y series does not fall on this line. This reflects the results in Figure 11 and Figure 13, where the increased total substitution on the B sites leads to increased ionic and electronic conductivities while all STCF-y series show identical behaviour, i.e. the substitution of Co increases ionic and electronic conductivities to the same extent.

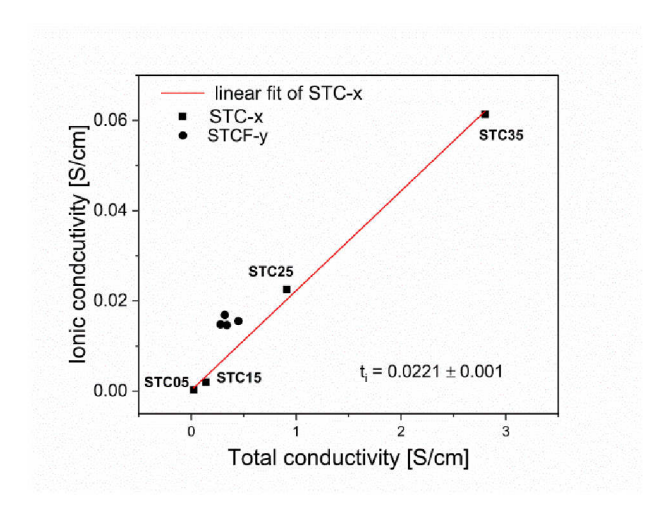


Figure 15 Ionic conductivity versus total conductivity of the STC-x and STCF-y series at 850 °C

In order to roughly investigate the long term stability of the oxygen permeation rate, more than 100 h of operation at 900 °C in lab conditions for STC25 and STF25 is shown in Figure 16. STC25 shows a slight initial decrease over the first 50 h and a stable performance for the remaining 70 h. In case of STF25 there is a larger scatter due to problems with the mass spectrometer. Nevertheless, there is no clear evidence of sever instability. However, in both cases more detailed analysis with longer times and measuring conditions, which are related to a targeted application, needs to be done.

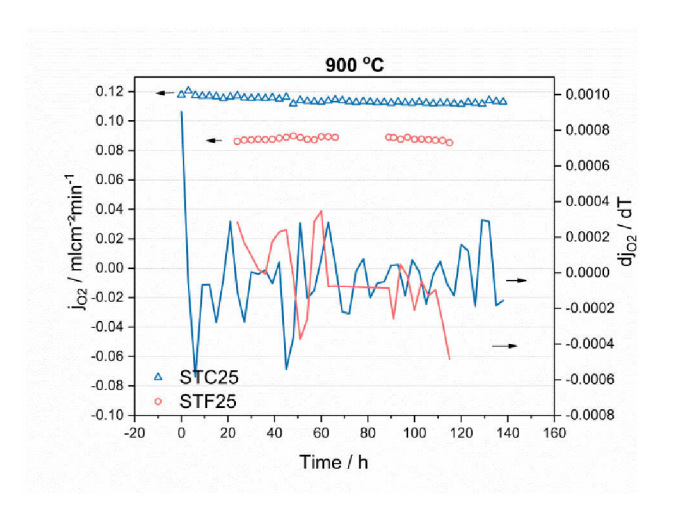


Figure 16. 100 h permeation rate of STC25 and STF25 samples of 1 mm thickness at 900 °C

Conclusions

We investigated the influence of the B-site substitution of SrTiO₃ with cobalt (STC) and iron (STCF) on properties relevant for application as an oxygen transport membrane, i.e. thermal/chemical expansion, electrical conductivity, and oxygen permeation rate.

As expected, cobalt on the B site leads to a functionalization in terms of inducing both electronic and ionic conductivities. For reasons of phase stability, the substitution level of cobalt should remain below 50%. On the other hand, significant conductivities can only be reached with a minimum substitution of 15%, since a sharp change in the dependence of the electronic conductivity and the ionic conductivity and, hence, the oxygen permeation rate on cobalt content can be observed at substitution level of 15% to 25%.

Therefore, if the substitution is in the range of 25-35%, the transport properties are promising. They are rationalised by the onset of percolation of Co–O bonds. The oxygen permeation rate is of the same order of magnitude as the state-of-the-art high-performance perovskite La_{0.6}Sr_{0.4}Co_{0.2}Fe_{0.8}O₃ (LSCF). Thermal and, in particular, chemical expansion remain relatively low compared to LSCF. This material therefore has great potential for utilization in oxygen transport membranes.

Compared to the B-site substitution of $SrTiO_3$ with iron (STF) and the solid solutions of both (STCF), it becomes apparent that for conditions where the solid-state diffusion is rate-limiting – in this case relatively thick membranes (1.0 mm) and high temperatures $\geq 800 \,^{\circ}\text{C}$ – cobalt shows no significant advantage over iron. Since the use of cobalt raises a number of economic, ecological and political/societal issues, STF can be viewed as a promising cobalt-free alternative in such cases.

At lower temperatures (≤750 °C) with an increasing influence of surface exchange kinetics, STC exhibits significantly higher oxygen flux compared to STF. Therefore, for application conditions in which surface exchange becomes rate-limiting, for example thin membranes and low temperatures or SOFC cathodes, the high catalytic activity of cobalt evidently leads to superior performance. It also appears that a mixture of Co and Fe is not very efficient. However, only a small number of data points are available, which is why more in-depth investigation on this matter is required.

Acknowledgements

We would like to thank the China Scholarship Council (CSC) for providing financial support for this work.

References

- [1] J. Sunarso, S. Baumann, J. Serra, W. Meulenberg, S. Liu, Y. Lin, J.D. Da Costa, Mixed ionic–electronic conducting (MIEC) ceramic-based membranes for oxygen separation, Journal of Membrane Science 320(1) (2008) 13-41.
- [2] A. Chroneos, R. Vovk, I. Goulatis, L. Goulatis, Oxygen transport in perovskite and related oxides: A brief review, Journal of Alloys and Compounds 494(1) (2010) 190-195.
- [3] F. Tietz, I.A. Raj, Q. Ma, S. Baumann, A. Mahmoud, R.P. Hermann, Material properties of perovskites in the Quasi-Ternary system LaFeO₃–LaCoO₃–LaNiO₃, Journal of solid state chemistry 237 (2016) 183-191.
- [4] A. Bedon, M.M. Natile, A. Glisenti, On the synthesis and stability of La_{0.6}Sr_{0.4}Ga_{0.3}Fe_{0.7}O₃, Journal of the European Ceramic Society 37(3) (2017) 1049-1058.
- [5] M. Burriel, C. Niedrig, W. Menesklou, S.F. Wagner, J. Santiso, E. Ivers-Tiffée, BSCF epitaxial thin films: Electrical transport and oxygen surface exchange, Solid State Ionics 181(13) (2010) 602-608.
- [6] L. Qiu, T. Lee, L.-M. Liu, Y. Yang, A. Jacobson, Oxygen permeation studies of SrCo_{0.8}Fe_{0.2}O_{3-δ}, Solid State Ionics 76(3-4) (1995) 321-329.
- [7] Y. Teraoka, T. Nobunaga, K. Okamoto, N. Miura, N. Yamazoe, Influence of constituent metal cations in substituted LaCoO₃ on mixed conductivity and oxygen permeability, Solid State Ionics 48(3-4) (1991) 207-212.
- [8] Z. Shao, S.M. Haile, A high-performance cathode for the next generation of solid-oxide fuel cells, Nature 431(7005) (2004) 170-173.
- [9] C. Niedrig, S. Taufall, M. Burriel, W. Menesklou, S.F. Wagner, S. Baumann, E. Ivers-Tiffée, Thermal stability of the cubic phase in Ba_{0.5}Sr_{0.5}Co_{0.8}Fe_{0.2}O_{3-δ} (BSCF) 1, Solid State Ionics 197(1) (2011) 25-31.
- [10] E.V. Artimonova, O.A. Savinskaya, A.P. Nemudry, Effect of B-site tungsten doping on structure and oxygen permeation properties of SrCo_{0.8}Fe_{0.2}O_{3-δ} perovskite membranes, Journal of the European Ceramic Society 35(8) (2015) 2343-2349.
- [11] M. Kuhn, S. Hashimoto, K. Sato, K. Yashiro, J. Mizusaki, Oxygen nonstoichiometry and thermo-chemical stability of La_{0.6}Sr_{0.4}CoO_{3-ō}, Journal of Solid State Chemistry 197 (2013) 38-45.

- [12] J. Ovenstone, J.-I. Jung, J.S. White, D.D. Edwards, S.T. Misture, Phase stability of BSCF in low oxygen partial pressures, Journal of Solid State Chemistry 181(3) (2008) 576-586.
- [13] S.J. Xu, W.J. Thomson, Stability of La_{0.6}Sr_{0.4}Co_{0.2}Fe_{0.8}O₃₋₅ perovskite membranes in reducing and nonreducing environments, Industrial & engineering chemistry research 37(4) (1998) 1290-1299.
- [14] M. Arnold, H. Wang, A. Feldhoff, Influence of CO_2 on the oxygen permeation performance and the microstructure of perovskite-type $(Ba_{0.5}Sr_{0.5})(Co_{0.8}Fe_{0.2})O_{3-\delta}$ membranes, Journal of Membrane Science 293(1) (2007) 44-52.
- [15] O. Ravkina, T. Klande, A. Feldhoff, Investigation of Zr-doped BSCF perovskite membrane for oxygen separation in the intermediate temperature range, Journal of Solid State Chemistry 201 (2013) 101-106.
- [16] F. Wang, T. Nakamura, K. Yashiro, J. Mizusaki, K. Amezawa, Effect of Nb doping on the chemical stability of BSCF-based solid solutions, Solid State Ionics 262 (2014) 719-723.
- [17] L. Bi, E. Fabbri, E. Traversa, Novel Ba_{0.5}Sr_{0.5}(Co_{0.8}Fe_{0.2})_{1-x}Ti_xO_{3- δ} (x= 0, 0.05, and 0.1) cathode materials for proton-conducting solid oxide fuel cells, Solid State Ionics 214 (2012) 1-5.
- [18] P. Haworth, S. Smart, J. Glasscock, J.D. Da Costa, Yttrium doped BSCF membranes for oxygen separation, Separation and Purification Technology 81(1) (2011) 88-93.
- [19] V. Cascos, L. Troncoso, J.A. Alonso, New families of Mn⁺-doped SrCo_{1-x}M_xO_{3-δ} perovskites performing as cathodes in solid-oxide fuel cells, International Journal of Hydrogen Energy 40(34) (2015) 11333-11341.
- [20] Y. Shen, F. Wang, X. Ma, T. He, $SrCo_{1-y}Ti_yO_{3-\delta}$ as potential cathode materials for intermediate-temperature solid oxide fuel cells, Journal of Power Sources 196(18) (2011) 7420-7425.
- [21] L.-S. Unger, R. Ruhl, M. Meffert, C. Niedrig, W. Menesklou, S.F. Wagner, D. Gerthsen, H.J.M. Bouwmeester, E. Ivers-Tiffée, Yttrium doping of Ba_{0.5}Sr_{0.5}Co_{0.8}Fe_{0.2}O_{3-δ} part II: Influence on oxygen transport and phase stability, Journal of the European Ceramic Society 38(5) (2018) 2388-2395.
- [22] L.-S. Unger, C. Niedrig, S.F. Wagner, W. Menesklou, S. Baumann, W.A. Meulenberg, E. Ivers-Tiffée, Yttrium doping of Ba_{0.5}Sr_{0.5}Co_{0.8}Fe_{0.2}O_{3-δ} part I: Influence on oxygen permeation, electrical properties, reductive stability, and lattice parameters, Journal of the European Ceramic Society 38(5) (2018) 2378-2387.
- [23] F. Schulze-Küppers, S. Ten Donkelaar, S. Baumann, P. Prigorodov, Y. Sohn, H. Bouwmeester, W. Meulenberg, O. Guillon, Structural and functional properties of $SrTi_{1-x}Fe_xO_{3-\delta}$

- $(0 \le x \le 1)$ for the use as oxygen transport membrane, Separation and purification technology 147 (2015) 414-421.
- [24] L.-W. Tai, M. Nasrallah, H. Anderson, D. Sparlin, S. Sehlin, Structure and electrical properties of La_{1-x}Sr_xCo_{1-y}Fe_yO₃. Part 1. The system La_{0.8}Sr_{0.2}Co_{1-y}Fe_yO₃, Solid State Ionics 76(3-4) (1995) 259-271.
- [25] V. Kharton, A. Yaremchenko, A. Kovalevsky, A. Viskup, E. Naumovich, P. Kerko, Perovskite-type oxides for high-temperature oxygen separation membranes, Journal of Membrane Science 163(2) (1999) 307-317.
- [26] V. Kharton, L. Shuangbao, A. Kovalevsky, A. Viskup, E. Naumovich, A. Tonoyan, Oxygen permeability and thermal expansion of SrCo(Ti)O_{3-δ} perovskites, Materials chemistry and physics 53(1) (1998) 6-12.
- [27] N. Xu, H. Zhao, Y. Shen, T. Chen, W. Ding, X. Lu, F. Li, Structure, electrical conductivity and oxygen permeability of $Ba_{0.6}Sr_{0.4}Co_{1-x}Ti_xO_{3-\delta}$ ceramic membranes, Separation and Purification Technology 89 (2012) 16-21.
- [28] T. Nagai, W. Ito, T. Sakon, Relationship between cation substitution and stability of perovskite structure in SrCoO_{3-δ}-based mixed conductors, Solid State Ionics 177(39) (2007) 3433-3444.
- [29] J. Tong, W. Yang, R. Cai, B. Zhu, G. Xiong, L. Lin, Investigation on the structure stability and oxygen permeability of titanium-doped perovskite-type oxides of $BaTi_{0.2}Co_xFe_{0.8-x}O_{3-\delta}$ (x=0.2–0.6), Separation and purification technology 32(1) (2003) 289-299.
- [30] S.-L. Zhang, H. Wang, M.Y. Lu, A.-P. Zhang, L.V. Mogni, Q. Liu, C.-X. Li, C.-J. Li, S.A. Barnett, Cobalt-substituted SrTi_{0.3}Fe_{0.7}O_{3-δ}: a stable high-performance oxygen electrode material for intermediate-temperature solid oxide electrochemical cells, Energy & Environmental Science 11(7) (2018) 1870-1879.
- [31] D. Fagg, V. Kharton, A. Kovalevsky, A. Viskup, E. Naumovich, J. Frade, The stability and mixed conductivity in La and Fe doped SrTiO 3 in the search for potential SOFC anode materials, Journal of the European ceramic Society 21(10) (2001) 1831-1835.
- [32] N.H. Perry, J.J. Kim, S.R. Bishop, H.L. Tuller, Strongly coupled thermal and chemical expansion in the perovskite oxide system $Sr(Ti, Fe)O_{3-\alpha}$, Journal of Materials Chemistry A 3(7) (2015) 3602-3611.
- [33] J. Jurado, F. Figueiredo, B. Gharbage, J. Frade, Electrochemical permeability of Sr_{0.7}(Ti, Fe) O_{3-δ} materials, Solid State Ionics 118(1) (1999) 89-97.
- [34] R. Oliveira Silva, J. Malzbender, F. Schulze-Küppers, S. Baumann, O. Guillon, Mechanical properties and lifetime predictions of dense $SrTi_{1-x}Fe_xO_{3-\delta}$ (x=0.25, 0.35, 0.5), Journal of the European Ceramic Society 37(7) (2017) 2629-2636.

- [35] J.P. Velev, K.D. Belashchenko, D.A. Stewart, M. van Schilfgaarde, S. Jaswal, E.Y. Tsymbal, Negative Spin Polarization and Large Tunneling Magnetoresistance in Epitaxial Co| SrTiO₃| Co Magnetic Tunnel Junctions, Physical review letters 95(21) (2005) 216601.
- [36] D. Yao, X. Zhou, S. Ge, Raman scattering and room temperature ferromagnetism in Codoped SrTiO₃ particles, Applied Surface Science 257(22) (2011) 9233-9236.
- [37] J. Lee, Z. Khim, Y. Park, D. Norton, N. Theodoropoulou, A. Hebard, J. Budai, L. Boatner, S. Pearton, R. Wilson, Magnetic properties of Co-and Mn-implanted BaTiO₃, SrTiO₃ and KTaO₃, Solid-State Electronics 47(12) (2003) 2225-2230.
- [38] K. Wongsaprom, E. Swatsitang, S. Maensiri, S. Srijaranai, S. Seraphin, Room temperature ferromagnetism in Co-doped La_{0.5}Sr_{0.5}TiO_{3-δ} nanoparticles, Applied physics letters 90(16) (2007) 162506.
- [39] J. Florez, S. Ong, M. Onbaşli, G. Dionne, P. Vargas, G. Ceder, C. Ross, First-principles insights on the magnetism of cubic $SrTi_{1-x}Co_xO_{3-\delta}$, Applied Physics Letters 100(25) (2012) 252904.
- [40] D.H. Kim, L. Bi, P. Jiang, G.F. Dionne, C. Ross, Magnetoelastic effects in SrTi_{1-x}M_xO₃ (M= Fe, Co, or Cr) epitaxial thin films, Physical Review B 84(1) (2011) 014416.
- [41] M.T. Colomer, A.L. Ortiz, V. López-Domínguez, J.M. Alonso, M.A. García, Preparation, thermal and phase evolution and functional properties of non-stoichiometric strontium-doped lanthanum manganite perovskite ceramics, Journal of the European Ceramic Society 37(11) (2017) 3527-3533.
- [42] C.W. Bezerra, L. Zhang, K. Lee, H. Liu, A.L. Marques, E.P. Marques, H. Wang, J. Zhang, A review of Fe–N/C and Co–N/C catalysts for the oxygen reduction reaction, Electrochimica Acta 53(15) (2008) 4937-4951.
- [43] Y. Teraoka, H. Zhang, K. Okamoto, N. Yamazoe, Mixed ionic-electronic conductivity of La_{1-x}Sr_xCo_{1-y}Fe_yO_{3-ō} perovskite-type oxides, Materials Research Bulletin 23(1) (1988) 51-58.
- [44] A.R. Denton, N.W. Ashcroft, Vegard's law, Physical review A 43(6) (1991) 3161.
- [45] S. Malo, A. Maignan, Structural, Magnetic, and Transport Properties of the $SrTi_{1-x}Co_xO_{3-\delta}$ Perovskite (0 \leq x \leq 0.9), Inorganic chemistry 43(25) (2004) 8169-8175.
- [46] R.D. Shannon, Revised effective ionic radii and systematic studies of interatomic distances in halides and chalcogenides, Acta crystallographica section A: crystal physics, diffraction, theoretical and general crystallography 32(5) (1976) 751-767.
- [47] S. Baumann, F. Schulze-Küppers, S. Roitsch, M. Betz, M. Zwick, E.M. Pfaff, W.A. Meulenberg, J. Mayer, D. Stöver, Influence of sintering conditions on microstructure and oxygen

- permeation of $Ba_{0.5}Sr_{0.5}Co_{0.8}Fe_{0.2}O_{3-\delta}$ (BSCF) oxygen transport membranes, Journal of Membrane Science 359(1) (2010) 102-109.
- [48] F. Schulze-Küppers, S. Baumann, F. Tietz, H.J. Bouwmeester, W. Meulenberg, Towards the fabrication of La_{0.98-x}Sr_xCo_{0.2}Fe_{0.8}O_{3-δ} perovskite-type oxygen transport membranes, Journal of the European Ceramic Society 34(15) (2014) 3741-3748.
- [49] Y. Xing, S. Baumann, D. Sebold, M. Rüttinger, A. Venskutonis, W.A. Meulenberg, D. Stöver, Chemical Compatibility Investigation of Thin-Film Oxygen Transport Membranes on Metallic Substrates, Journal of the American Ceramic Society 94(3) (2011) 861-866.
- [50] H.J. Park, G.M. Choi, Oxygen permeability of gadolinium-doped ceria at high temperature, Journal of the European Ceramic Society 24(6) (2004) 1313-1317.
- [51] Y. Teraoka, T. Nobunaga, K. Okamoto, N. Miura, N. Yamazoe, Influence of constituent metal cations in substituted LaCoO₃ on mixed conductivity and oxygen permeability, Solid State Ionics 48(3) (1991) 207-212.
- [52] A. Rothschild, W. Menesklou, H.L. Tuller, E. Ivers-Tiffee, Electronic Structure, Defect Chemistry, and Transport Properties of SrTi_{1-x}Fe_xO_{3-y} Solid Solutions, Chemistry of Materials 18(16) (2006) 3651-3659.
- [53] K. Zhang, L. Ge, R. Ran, Z. Shao, S. Liu, Synthesis, characterization and evaluation of cation-ordered LnBaCo₂O_{5+δ} as materials of oxygen permeation membranes and cathodes of SOFCs, Acta Materialia 56(17) (2008) 4876-4889.
- [54] s. Steinsvik, r. Bugge, j. Gjønnes, j. Taftø, t. Norby, The defect structufe of SrTi_{1-x}Fe_xO_{3-y} (x=0-0.8) investigated by electrical conductivity measurements and electron energy loss spectroscopy (EEIS), Journal of Physics and Chemistry of Solids 58(6) (1997) 969-976.
- [55] T. Ishihara, T. Yamada, H. Arikawa, H. Nishiguchi, Y. Takita, Mixed electronic—oxide ionic conductivity and oxygen permeating property of Fe-, Co-or Ni-doped LaGaO 3 perovskite oxide, Solid State Ionics 135(1) (2000) 631-636.
- [56] Z. Chen, R. Ran, W. Zhou, Z. Shao, S. Liu, Assessment of $Ba_{0.5}Sr_{0.5}Co_{1-y}Fe_y$ $O_{3-\delta}$ (y= 0.0–1.0) for prospective application as cathode for IT-SOFCs or oxygen permeating membrane, Electrochimica Acta 52(25) (2007) 7343-7351.
- [57] M. Patrakeev, A. Markov, I. Leonidov, V. Kozhevnikov, V. Kharton, Ion and Electron Conduction in $SrFe_{1-x}Sc_xO_{3-\delta}$, Solid State Ionics 177(19) (2006) 1757-1760.
- [58] W. Koros, Y. Ma, T. Shimidzu, Terminology for membranes and membrane processes, J. Membr. Sci 120(2) (1996) 149-159.
- [59] C. Argirusis, F. Jomard, S.F. Wagner, W. Menesklou, E. Ivers-Tiffée, Study of the oxygen incorporation and diffusion in Sr(Ti_{0.65}Fe_{0.35})O₃ ceramics, Solid State Ionics 192(1) (2011) 9-11.

- [60] Y. Wang, J. Ren, Y. Wang, F. Zhang, X. Liu, Y. Guo, G. Lu, Nanocasted synthesis of mesoporous LaCoO₃ perovskite with extremely high surface area and excellent activity in methane combustion, The Journal of Physical Chemistry C 112(39) (2008) 15293-15298.
- [61] A. Glisenti, M. Natile, S. Carlotto, A. Vittadini, Co-and Cu-Doped Titanates: Toward a New Generation of Catalytic Converters, Catalysis letters 144(8) (2014) 1466-1471.
- [62] W. Jung, H.L. Tuller, Impedance study of $SrTi_{1-x}Fe_xO_{3-\delta}$ (x= 0.05 to 0.80) mixed ionic-electronic conducting model cathode, Solid State Ionics 180(11) (2009) 843-847.
- [63] Y. Yamamura, S. Kawasaki, H. Sakai, Molecular dynamics analysis of ionic conduction mechanism in yttria-stabilized zirconia, Solid State Ionics 126(1) (1999) 181-189.
- [64] S. Molin, W. Lewandowska-Iwaniak, B. Kusz, M. Gazda, P. Jasinski, Structural and electrical properties of Sr(Ti, Fe)O_{3-δ} materials for SOFC cathodes, Journal of electroceramics 28(1) (2012) 80-87.
- [65] H. Hayashi, H. Inaba, M. Matsuyama, N. Lan, M. Dokiya, H. Tagawa, Structural consideration on the ionic conductivity of perovskite-type oxides, Solid State Ionics 122(1) (1999) 1-15.